# Adsorptive potential of synthesized sea urchin-based hydroxyapatite for Supranol yellow and nickel ion recovery from aqueous media: kinetics and thermodynamic studies

Aicha Medjdoub, Fadila Nemchi, Hanane Belayachi, Benaouda Bestani*, Sarra Bourahla, Mostefa Belhakem, Nouredine Benderdouche

*Laboratoire de Structure, Elaboration et Application de Matériaux Moléculaires, SEAMM, Faculté des sciences et de la technologie, Université Abdelhamid Ibn Badis – Mostaganem, Algéria, emails: bestanib@yahoo.fr (B. Bestani), medjdoubaicha@yahoo.com, (A. Medjdoub), delanemchi@yahoo.fr (F. Nemchi), belayachi.hanane@hotmail.fr (H. Belayachi), sarra.bourahla@univ-mosta.dz (S. Bourahla), mbelhakem@hotmail.com (M. Belhakem), benderdouchen@yahoo.fr (N. Benderdouche)*

## ABSTRACT

Locally affordable, eco-friendly and non-toxic biomaterial, sea urchin test (*Paracentrotus lividus*) as a precursor was converted in this investigation by simple and viable way into an efficient adsorbent for nickel ions and Supranol yellow dye removal from simulated wastewater. Powered urchin shell sea urchin test (SUT) and diammonium phosphate as sources of calcium and potassium, respectively, were used for hydroxyapatite synthesis by chemical precipitation route followed by calcination at 800°C. The resulting calcium phosphate based-adsorbent: hydroxyapatite urchin test (HAP-UT) was characterized by Fourier-transform infrared spectroscopy, X-ray diffraction, Brunauer–Emmett–Teller and $pH_{zpc}$ to appraise its physicochemical characteristics as well as the mechanism of both pollutants adsorption. Effect of conventional parameters on both pollutants uptakes such as equilibrium time, adsorbent dose, pH and temperature were also performed. Well known adsorption isotherms, namely Langmuir and Freundlich were used for data fitting to describe the adsorption equilibrium of both pollutants The raw material conversion to HAP-UT enhances the removal capacities from 58.48 to 666.67 mg g$^{-1}$ at pH 2–3 and from 1.49 to 29.50 mg g$^{-1}$ at pH 5–5.4 for Yellow supranol and nickel ions respectively. From the perspective of higher $R^2$ values and the lower root mean square error values as an error indicator, Langmuir model is more representative for the experimental data predicting homogeneous surface coverage of the adsorbents. Thermodynamic analysis of the adsorption processes of both pollutants confirms their spontaneity and endothermicity. Adsorption mechanism found to obey to pseudo-second-order kinetic model. Obtained results showed that the synthetized hydroxyapatite from urchin shell as an adsorbent could prove to be very useful and efficient in removing toxic pollutants from industrial effluents.

*Keywords: Paracentrotus lividus*; Simulated-wastewater; Removal; Toxic pollutants

## 1. Introduction

Nowadays, significant amounts of dyes and heavy metals compounds-laden wastewater are produced by many industries from which effluent discharge constitutes the main source of the environment pollution leading to negative impact on human lives, public health and soil contamination [1].

Firstly, it has been an increasing ecological and public health concern associated with environmental contamination

* Corresponding author.

by heavy metals. Even at lower concentrations, they are not easily biodegraded, they can persist in the environment for a long period of time and become harmful by developing their toxicity by bioaccumulation. Human exposure has risen dramatically as a result of their increase use in several industrial, agricultural and technological applications and other point source areas such as mining, smelters and other metal-based industrial operations [2,3]. Nickel among heavy metals, occurs naturally in the environment at low levels and can be found in food (mainly in plants) non-food sources (coins, glasses frame and various household appliances) [4]. The major sources of nickel contamination in soils, groundwater and surface water are metal plating industries, fossil fuels combustion, nickel mining, alloy products and electroplating, in which nickel occurs at higher levels becoming then a toxic element and causing chronic effects such as dermatitis, eczema, asthma, lungs and immune system from inhalation and exposure.

Secondly, a variety of dyestuffs is extensively used in many industrial branches such as textile, printing and paints [5]. Most of them are resistant to environmental conditions and hardly biodegradable in conventional wastewater treatment plants due to their complex aromatic structures. Among them, Supranol yellow which is an acid dye of the disazo series. Its industrial uses include the dyeing of paper and leather as well as the colouring of cellulose acetate in injection moulding. Both types of pollutants considered in this study and many others can degrade into highly carcinogenic toxic products and can be harmful. So, their removal from wastewater before their release to the environment is extremely important.

Therefore, a variety of methods have been developed for removing dyes and heavy metals compounds from wastewaters; among them adsorption on solid adsorbents become one of the most effective method [6,7] and has received increasing attention by scientists in recent years as for removing a wide range of pollutant-laden effluents.

Among a large variety of materials-based adsorbents that have been developed for these purposes such as montmorillonite, algal species and all types of agro wastes [8–11], hydroxyapatite and its derivative forms have emerged as excellent biomaterials that recently gained attention as efficient adsorbents. It is also characterized by its high chemical and thermal stability, its great power of ion exchange and the disponibility of raw materials that can be used for its synthesis [12].

Hydroxyapatite can be produced by different ways such as hydrothermal, solvo-thermal and chemical precipitation methods [13]. The chemical precipitation route was chosen in this study as a suitable method for hydroxyapatite synthetizes from sea urchin test, a raw and costless material largely available used as a potential source of calcium [Ca], and $(NH_4)_2PO_4$ (diammonium phosphate) as a source of phosphorus [P]. The obtained hydroxyapatite-based sea urchin shell adsorbent was used for nickel ions and Supranol yellow removal from simulated wastewater. As reported in the literature, many studies reported the use of this material for heavy metals and dyes removal [14–20].

## 2. Materials and methods

### 2.1. Chemicals and reagents

All chemicals used in this study were of analytical grade. Supranol yellow was used in this study as received, nickel chloride hexahydrate (99.9%), diammonium hydrogen phosphate $((NH_4)_2HPO_4)$ 98% and dimethylglyoxime (DMG), >99% (Sigma-Aldrich, Germany). Stock soloutions were prepared according to standard procedure. A $10^{-3}$ M, solution of nickel by dissolving 0.2377 g of $NiCl_2 \cdot 6H_2O$ in 1 L of doubly distilled water (corresponding to 0.0587 g of $Ni^{2+}/L$) and 1.0 g $L^{-1}$ of Supranol yellow solution. Working solutions of the desired concentrations were obtained by successive dilutions. Some major characteristics of the main chemicals used in this study are summarized in Table 1.

Widely used for the spectrophotometric determination of microamounts of nickel in solution, DMG gives with nickel a distinct coloured complex solution. A 2.5% solution was prepared by dissolving 2.5 g of DMG in 100 mL of ethanol. Buffer solutions were prepared by mixing suitable amounts of 1 M acetic acid and 1 M ammonium acetate solution at pH 3–6, or 1 M ammonia water and 1 M ammonium acetate solution at pH 8–11. To 15 mL of the solution in 0.5 M HCl medium containing a certain amount of Ni(II), were added 2 mL of DMG (2.5%), 1 mL of 10 M sodium hydroxide and 0.3 mL of ammonium persulfate (10% in water). After 10 min, the volume was completed to 25 mL and measures were taken at 460 nm for nickel concentration determination [21,22]. In order to validate this analytical method, two important and commonly terms are used to describe the smallest concentration of an analyte that can be reliably measured by an analytical procedure: They are the limit of detection (LoD) given by: LoD = $[3.3 \times (\sigma/s)]$ estimated from replicates of large number of blanks and the limit of quantification (LoQ) given by: LoQ = $[10 \times (\sigma/s)]$, where ($\sigma$) is the standard deviation of the response and

Table 1
Chemical structure and characteristics of reagents used in this study

|  | Diammonium phosphate | Nickel | Supranol yellow |
|---|---|---|---|
| CAS number | 7783-28-0 | 7791-20-0 | 8005-52-5 |
| Chemical formula | $(NH_4)_2HPO_4$ | $NiCl_2 \cdot 6H_2O$ | $C_{16}H_{10}N_2O_7S_2Na_2$ |
| Provided by | Panreac Montplet & Esteban, SA-Spain | Riedel-deHaën, Germany | Ciba Society, Switzerland |
| Molecular weight (g $mol^{-1}$) | 132.07 | 237.69 | 452.0 |
| Max. wavelength $\lambda_{max}$ (nm) | // | 465 | 405 |
| Solubility (g $L^{-1}$) | 106.7 g/100 mL (100°C) | Highly soluble | 120 (@90°C) |

(*s*) is the slope of the calibration curve. The coefficients 3.3 and 10 in the above equations are called expansion factors and are obtained assuming a 95% confidence level. Both limits were evaluated from the calibration curves of nickel and Yellow supranol obtained from the absorbance vs. concentration plots represented by straight lines, validating then the Lambert–Beer's law ($A = \epsilon LC$) in the chosen concentration range using Excel software.

## 2.2. Adsorbents preparation

Due to its abundance on the Mostaganem area-Algeria (South Mediterranean coast), sea urchin test (*Paracentrotus lividus*) as a raw material with a high content of calcium carbonate was selected and converted into hydroxylamine by precipitation method followed by calcination at 800°C. The obtained material was used as an adsorbent for nickel ions and Supranol yellow dye removal from aqueous solutions. The raw material was first washed with tap water to remove dust and other impurities then with distilled water and dried at 70°C overnight, grinded, sieved through 0.071 mm using a jar mill (Vierzen grinder) before pollutants removal tests. A amount of 20 g of the sea urchin test material (calcium source) were introduced into a beaker containing 14 g of $(NH_4)_2HPO_4$ initially dissolved in 50 mL of distilled water. The mixture was vigorously stirred at ambient for 72 h, then stabilized and adjusted to pH 12 by adding $NH_4OH$ solution, filtered and rinsed with distilled water to neutral, oven dried overnight at 60°C, then grinded and sieved. The resulting material is then pyrolyzed at 800°C for 3 h in tubular furnace (Nabertherm MORETHAN HEAT 30-3,000°C). The obtained fine powder is again washed with distilled water, in order to dissolve the CaO content, until neutral pH then oven died for 24 h at 60°C and kept in desiccators before adsorption tests.

## 2.3. Adsorbent characterization

### 2.3.1. Surface area

Nitrogen at 77 K was used for surface area determination using an automated adsorption apparatus (Micromeritics apparatus ASAP 2020). Prior to analysis, prepared adsorbents were degassed at 150°C in a vacuum system at low pressure ($10^{-4}$ torr). The specific surface area ($S_{BET}$) was determined using the Brunauer–Emmett–Teller (BET) isotherm model in the region of relative pressures near completed monolayers ($0.05 < P/P_0 < 0.3$), with $N_2$ cross-sectional area equals to $16.2 \cdot 10^{-20}$ m².

### 2.3.2. Zero point of charge ($pH_{zpc}$) determination

Depending of the adsorbent surface charge (adsorption at low pH means net positive charge due to $H^+$ presence and its liberation at high pH means net negative charge). The absence of both charges implying that the net charge is zero also called zero point of charge ($pH_{zpc}$) is a key parameter in adsorbent surface [23].

In other words, if $pH < pH_{zpc}$, the surface charge of adsorbent would be positive so that the anionic species are favorably adsorbed, and the cationic species are favorably adsorbed at $pH > pH_{zpc}$. The $pH_{zpc}$ is generally determined from ($\Delta pH = pH_i – pH_f$) vs. ($pH_i$) plot as reported in previous work [24].

### 2.3.3. Identification of crystalline phases

In order to identify the phase composition of the prepared samples and to highlight their equidistance, crystalline phases identification was performed examined by means of X-ray diffraction (XRD: Bruker P8 Advance technique) with a 2 h range of 20–60 in 0.02 steps and powder diffraction files was used for patterns identification.

### 2.3.4. Fourier-transform infrared spectroscopy

Fourier-transform infrared (FT-IR) spectrometer Perkin Elmer employing KBr pellet method in the range of 4,000–400 cm⁻¹ was used for samples surface functional groups identification. Samples of 1 mg of dried and finely grinded activated carbon were thoroughly mixed with 100 mg of KBr and compressed in order to make a thin film disk for spectra analysis.

## 2.4. Batch uptakes studies of Supranol yellow and nickel ions

The batch adsorption studies of both pollutants on hydroxyapatite urchin test (HAP-UT) and sea urchin test (SUT) samples were carried out at different parameters affecting adsorption rate such as pH in the range of 2–12, initial concentration ranging from 100 to 1,000 mg L⁻¹ for Supranol yellow (4GL) and from 0.5869 to 5.869 mg L⁻¹ for Ni²⁺, contact time ranging from 30 to 280 min, adsorbent dose ranging from 2–20 g L⁻¹ and three different temperatures of 293, 298 and 303 K. Experiments were performed by mixing an optimum dose of 0.4 g L⁻¹ of adsorbent (initially chosen on the basis that it was the dosage giving a high removal % in parameters affecting adsorption rate section) and 25 mL of chosen pollutant solutions of known concentration in 200 mL stoppered conical flasks. The resulting suspension was then agitated magnetically at a constant speed of 150 rpm at ambient till equilibrium then centrifuged at 4,000 rpm for 15 min. The supernatants were analyzed by spectrophotometry at $\lambda_{max}$ = 405 nm for the remaining Supranol yellow concentrations determination. DMG (2.5%) at $\lambda_{max}$ = 465 nm was adopted to measure Ni²⁺ concentrations remaining in solutions. Experiments were repeated in triplicate and the average values were reported for further calculations. According to mass balance relationship represented by Eq. (1), the adsorbed amount ($q_e$) was evaluated:

$$q_e = \frac{V}{m}\left(C_0 - C_{eq}\right) \tag{1}$$

where $C_0$ and $C_{eq}$ are the initial and the equilibrium nickel or Yellow supranol concentrations (mg L⁻¹) respectively, $V$ is the volume of the solution (L) and $m$ is the mass of the adsorbent (mg).

## 2.5. Modeling of adsorption isotherms

Solid–liquid phase concentrations plots were used to describe the equilibrium adsorption isotherm of Ni²⁺ ions

and Supranol yellow onto (HAP-UT and SUT). Two most commonly used adsorption isotherms equations have been tested in the present work to fit the experimental data, namely:

Langmuir model which assumes that the adsorption takes place at specific homogeneous sites within the adsorbent with no further adsorption taking place at the same site once filled is given by Eq. (2).

$$q_e = \frac{bK_L C_e}{1 + K_L C_e} \qquad (2)$$

where $q_e$ is amount of solute adsorbed per unit weight of adsorbent (mg g$^{-1}$), $C_{eq}$ is the concentration of solute remaining in solution at equilibrium (mg L$^{-1}$), $b$ (mg g$^{-1}$) is the maximum adsorption capacity corresponding to complete monolayer coverage and $K_L$ is a constant related to the energy or net enthalpy.

Freundlich model usually used to describe adsorption experiments taking place on heterogeneous adsorbent surface is given by Eq. (3),

$$q_e = K_F C_{eq}^{1/n} \qquad (3)$$

where $K_F$ and $n$ are the Freundlich constants related to adsorption capacity and adsorption intensity respectively.

### 2.6. Thermodynamic study

#### 2.6.1. Van't Hoff equation

The characteristics of the adsorption process of both pollutants such as spontaneity, nature and the adsorbent applicability, were determined using thermodynamic functions such as changes in the standard free energy ($\Delta G°$), the enthalpy ($\Delta H°$) and entropy ($\Delta S°$) were evaluated graphically from van't Hoff equation as functions of temperature and the adsorption distribution coefficient ($K_d$) using the following equations [25]:

$$K_d = \frac{q_e}{C_e} \quad \text{in} \quad \left( \text{Lg}^{-1} \right) \qquad (4)$$

$$\ln K_d = \frac{\Delta S°}{R} - \frac{\Delta H°}{T} \qquad (5)$$

$$\Delta G° = -RT \ln K_d = T\Delta S° - \Delta H° \qquad (6)$$

$$S^* = \left(1 - \theta\right) e^{\frac{-E_a}{RT}} \qquad (7)$$

$$\ln S^* = \ln\left(1 - \theta\right) - \frac{E_a}{RT} \qquad (8)$$

where $C_e$ and $C_i$ are respectively the residual and the initial concentrations of Ni$^{2+}$ or 4GL in the aqueous solutions (mg L$^{-1}$).

#### 2.6.2. Modified Arrhenius-type equation

Activation energy ($E_a$) and sticking probability ($S^*$) are two other parameters of important utility that can be estimated from the experimental data to support the adsorption mechanism predominance [26]. The relationships between the above-mentioned parameters and the surface coverage: $\theta = (1 - C_e/C_i)$ are given by the modified Arrhenius-type Eqs. (7) and its linearized form (8).

## 3. Results and discussion

### 3.1. Sample characterization

#### 3.1.1. Surface area

The pore structure characterization of both adsorbents (SUT and HAP-UT) was carried out using the BET method (N$_2$ adsorption isotherms at 77 K). Their textural characteristics are shown in Table 1 and their N$_2$ adsorption/desorption isotherms as a function of specified relative pressure ($P/P_0$) are shown in Fig. 1. The N$_2$ adsorption-desorption isotherm of HAP-UT sample exhibits type IV isotherm, which is typical of mesoporous materials, with H3 type hysteresis loop associated to capillary condensation defined by IUPAC [27]. As illustrated in Fig. 1, the adsorption amount increases quiet rapidly in the relatively low-pressure region ($P/P_0 < 0.03$), which indicates the presence of micropores. After the filling of the later, a gradual increase of N$_2$ adsorption reflecting monolayer to multilayer adsorption process is observed. At $P/P_0 > 0.98$, slight capillary condensation of N$_2$ occurs in larger mesopores and macropores indicated by the large mesoposous volume of 0.227 cm$^3$g$^{-1}$ compared to the total volume of 0.235 cm$^3$ g$^{-1}$ (Table 2). HAP-UT sample shows also broader hysteresis loop covering the range from $P/P_0 = 0.30$ to 0.99.

As expected, the untreated material (SUT) has very low specific area of 0.1836 m$^2$ g$^{-1}$ (Table 1), this is due to pores clogging by the presence of minerals and organics. In contrast, hydroxyapatite-based adsorbent (HAP-UT) synthesized by the adopted simultaneous treatment has enhanced significantly the surface area of up to 87.36 m$^2$ g$^{-1}$ by evacuating all the impurities and organics, thus creating more internal porous space.
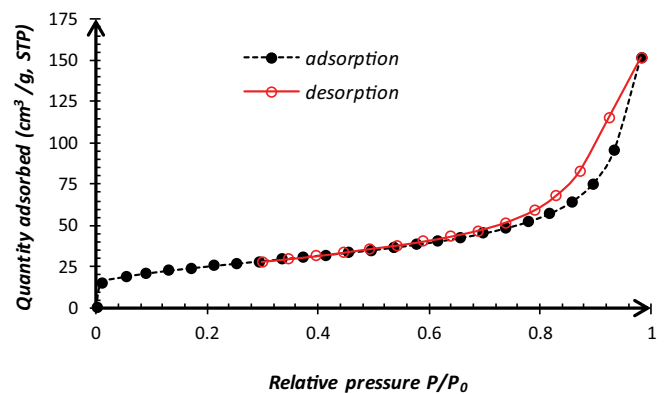


Fig. 1. Adsorption–desorption isotherms of N$_2$ at 77 K onto HAP-UT sample.

Table 2
Textural characteristics of HAP-UT and SUT samples obtained by N$_2$ adsorption–desorption analysis

| Properties | Adsorbants | |
|---|---|---|
| | SUT | HAP-UT |
| BET specific surface area (m$^2$ g$^{-1}$) | 0.184 | 87.36 |
| Total volume (cm$^3$ g$^{-1}$) | // | 0.235 |
| Mesoporous volume (cm$^3$ g$^{-1}$) | // | 0.227 |
| Mean pore diameter (nm) | // | 8.10 |
| pH$_{zpc}$ | 8.0 | 8.2 |

### 3.1.2. pH of zero point charge (pH$_{zpc}$)

Being an important parameter to predict the affinity of the adsorbent–adsorbate, pH value at which an adsorbent surface is globally neutral called the point of zero charge (pH$_{zpc}$) has been determined for both considered samples. At pH < pH$_{zpc}$: the adsorbent surface is positively charged attracting anionic substances, while it is negatively charged attracting then cationic substances at pH > pH$_{zpc}$. The obtained pH$_{zpc}$ values for both HAP-UT and SUT were 8.2 and 8.0 respectively determined graphically by the intersection point of pH$_{final}$ vs. pH$_{initial}$ plots (figure not shown).

Yellow supranol as an anionic dye was removal at the rate of 666.67 and 58.48 mg g$^{-1}$ respectively by a positively charged HAP-UT and SUT in the acidic media (pH range of 2.0–3.0) in conformity with the obtained pH$_{zpc}$ value (pH < pH$_{zpc}$: attraction between dye molecule and the adsorbent surface). In the other hand, nickel ions were removed effectively at the rate of 29.50 mg g$^{-1}$ by HAP-UT (pH = 5.4) and 1.49 mg g$^{-1}$ by SUT (pH = 5.0). For lower pH values the Ni(II) removal rate decreases to the presence of H$^+$. At pH values above 8.0, nickel mainly precipitated as Ni(OH)$_2$. Therefore, the observed removal in the later case was attributed not to adsorption but to precipitation.

### 3.1.3. Fourier-transform infrared spectroscopy

As an interferometric method, FT-IR spectroscopy is used in this study for samples surface functional groups identification. (Fig. 2) displays three main spectral regions for SUT and HAP-UT samples (hydoxyl: 3,800–3,200 cm$^{-1}$, carbonates: 1,600–1,200 cm$^{-1}$ and phosphates 1,100–500 cm$^{-1}$). (NH4)$_2$HPO$_4$ application to sea urchin raw material induces the appearance of new functional groups, such as peaks detected at 1,093 and 1,047 cm$^{-1}$ which may be ascribed to the doubly degenerate, υ3 asymmetric vibration modes of the P=O of the PO$_4^{3-}$ group and P–O–C which are responsible for the surface structure transformation of the synthesized sample. The bands at 607 and 560 cm$^{-1}$ and also 1,093 cm$^{-1}$ are generated by fundamental vibrational modes of PO4 species. Bands at 1,474 and 1,417 cm$^{-1}$ appeared in both samples, that can be attributed to carbonate groups replacing PO$_4^{3-}$ groups. However, heat treatment causes the disappearance of many functional groups ranging from 3,463 to 1,474 cm$^{-1}$ creating then more space into HAP-UT sample. In summary, the measured IR spectra analysis shows a variety of spectra of a broad and medium bond and other fine and medium one.
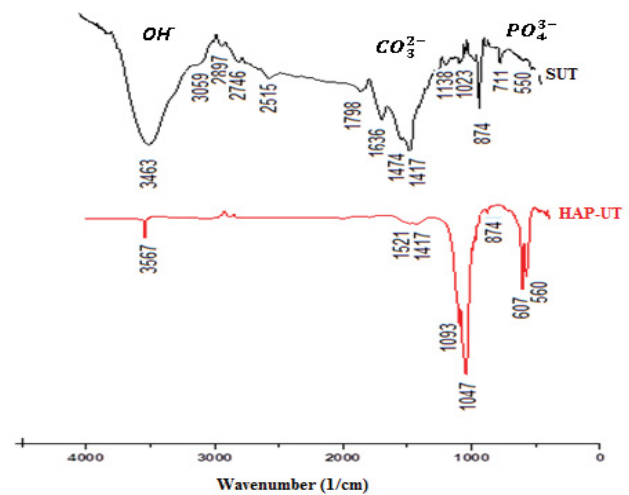


Fig. 2. FT-IR spectra of SUT and HAP-UT samples.

### 3.1.4. Crystalline phases identification

The diffractograms of calcite (SUT) and hydroxyapatite (HAP-UT) are shown in (Fig. 3). Their XRD data was processed X'Pert HighScore for miller indices and elemental mesh parameters determination of each material. According to XRD data, all characteristic peaks of SUT and HAP-UT are present. The decrease in their signal intensities or disappearance of some SUT peaks after conversion to HAP-UT are clearly shown in the same (Fig. 3).

The changes of SUT sample miller index' characteristic peaks are due to the change of the crystal system or calcite which is a represented by a Rhombohedron one with $a = b = 4.994$, $c = 17.081$ and a space group R-3C, while HAP-UT sample is represented by a hexagonal system with $a = b = 9.49$, $c = 6.85$ and a space group P63/m obtained from the referenced peaks of ICSD PAH 01-086-0740 database [28]. The low crystallinity rate of the synthesized material (HAP-UT) can be explained by the difference of peaks intensities. Moreover the substitution in carbonated B-type site induces a reduction of the crystallinity and the size of the obtained HAP-UT particles. Same findings were reported in the literature [29].

Also shown in Fig. 3, that the most intense and sharpest peaks are observed in the 2Ø angle range between 25Ø and 50Ø, coinciding with the XRD reference lines, which corresponds to HAP-UT crystals that are in good agreement with the JCPDS Card 09-0432 data (hydroxyapatite standard) [30,31].

## 3.2. Effect of conventional parameters on adsorption

Considered to affect considerably adsorption processes, the adsorbent dosage, equilibrium time, solution pH and temperature were studied prior to both pollutants uptakes onto SUT and HAP-UT for their optimal values determination.

### 3.2.1. Effect of adsorbent dose

Used for the treatment cost prediction of solid per unit of pollutant solution, the adsorbent dosage is an important

parameter in the sorbent–sorbate equilibrium determination. The dependence of both pollutants uptakes on the amount of SUT and HAP-UT was studied within the range of 2–20 g L$^{-1}$, maintaining all other parameters constant. As shown in (Fig. 4a), removal rate increases for 4GL dye with increasing dosage over the range 0–20 g L$^{-1}$ due the available sites. As shown in (Fig. 4a), maximum uptakes occurred for 4GL dye onto HAP-UT and SUT adsorbents respectively at the dose of 6 and 10 g L$^{-1}$. The same phenomena happened with Ni$^{2+}$ ions and maximum amount removed occurred at dosage of 20 g L$^{-1}$ for HAP-UT and SUT respectively for solution concentration of 14 mg L$^{-1}$.

### 3.2.2. Effect of solution pH

External solution pH greatly affects the adsorption process of the 4GL and Ni$^{2+}$, either by changing the adsorbents surface charge or by changing the dyes or the metal behavior for a special application, while controlling pollutants removal from liquid phase. In order to determine the optimum pH conditions for the both pollutants onto SUT and HAP-UT adsorbents, initial pH of the solution of known volume and concentration was placed in a beaker and was adjusted from 2 to 12 by adding either dilute NaOH or HCl (0.1 N) solutions. Then a certain volume of this solution was placed in a flask to which a certain amount of adsorbent (20 g L$^{-1}$: dose determined previously) was added and the mixture, shaken then filtered and the equilibrium concentration was determined by spectrophotometry for 4GL at $\lambda_{max}$ = 405 and Ni$^{2+}$ ions at $\lambda_{max}$ = 465. It can be seen from (Fig. 4b) that the adsorption of 4GL dye decreased from when the pH was increased from acidic media (pH = 2) to basic media (pH = 12). This fact could be explained that at lower pH, the overall surface area of the charge of both
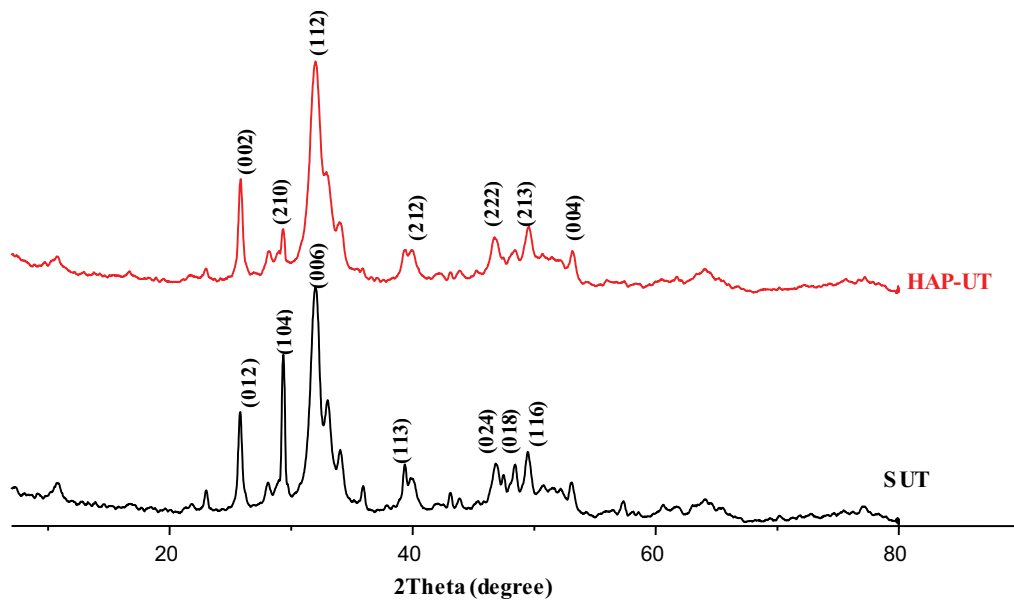


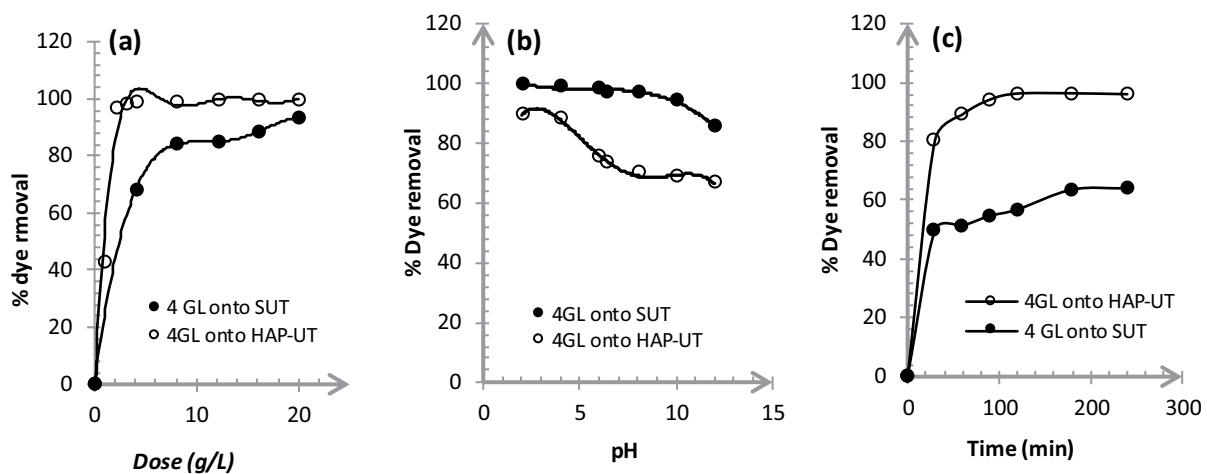Fig. 3. XRD patterns of synthetic hydroxyapatite (HAP-UT) and raw material (SUT).



Fig. 4. Effect of conventional parameters on 4GL adsorption: (a) adsorbent dosage, (b) pH and (c) equilibrium time (conditions: $T$ = 25°C ± 0.1°C, $C_0$ = 100 mg L$^{-1}$).

materials (SUT) and (HAP-UT) is positive ($pH_{zpc} \sim 8.2$), which favors the adsorption of 4GL as an anionic dye by attraction (electrostatic forces), otherwise the adsorption of anionic species is favored at $pH < pH_{zpc}$ [8,32].

In the other hand, $Ni^{2+}$ uptake was favoured at pH 5–6, where removal rates were reached by HAP-UT and SUT respectively (Figure not shown). At lower pH values (2–4), higher $[H^+]$ exist in the solution (strong acid environment) protonating then to adsorbents surface functional groups resulting in lower $Ni^{2+}$ uptake. By increasing pH values, deprotonation takes place by decreasing $[H^+]$ (week acid environment) implying less competition between $H^+$ and $Ni^{2+}$, favouring the adsorption of the later. At higher pH > 7.5, $Ni^{2+}$ ions will precipitate into nickel hydroxide dropping then the removal rate. The pH optimal value of 5.4 for all experiments was chosen as it corresponds to the maximum uptakes of both pollutants by both samples. The same phenomena was reported for nickel ions uptake using different adsorbents [33–35].

### 3.2.3. Effect of contact time

The effect of equilibrium time of 4GL adsorption capacities onto HAP-UT and SUT samples is shown in Fig. 4c. It was found that the percentage removal of both pollutants increases rapidly with increasing time up to 40 min then slow down and finally stabilize when equilibrium is reached corresponding to 60 min for 4GL dye and 180 min for $Ni^{2+}$ ions adsorption. As a consequence, subsequent adsorption experiments were allowed to equilibrium for time periods in excess of these values, which were assumed to be largely ample for performing all experiments.

### 3.3. Adsorption isotherms

Both adsorption isotherms onto the investigated adsorbents at working conditions determined previously such as pH, adsorbent dosage, equilibrium time and temperature shown in Fig. 5 in their linear forms were fitted to experimental data and to describe the adsorption of $Ni^{2+}$ ions and 4GL dye at the solid–liquid interface. As it can be seen from Fig. 5a and b that the uptake rates increase rapidly due to the availability of sites for low concentrations in solution then attenuates to reach a plateau (saturation sites) corresponding to maximum adsorption capacities values of both pollutants evaluated from Langmuir isotherm and presented in Table 3.

The Langmuir equilibrium parameter $R_L$ indicate that adsorption processes were carried out favorably since all values are $0 < R_L < 1$ values for all samples which is in agreement with the adsorption intensity factor $n > 1$ derived from Freundlich model which states that the magnitude of $n$ depicts the adsorption process favorability, with $2 < n < 10$ (very favorable), $1 < n < 2$ (moderately difficult) and $n < 1$ (poor adsorption potential). The $n$ values obtained from Fig. 6a and reported in Table 3 are >2 meaning that the adsorption processes for 4GL dye by HAP-T

Table 3
Langmuir and Freundlich parameters for 4GL and $Ni^{2+}$ removal onto the prepared adsorbents

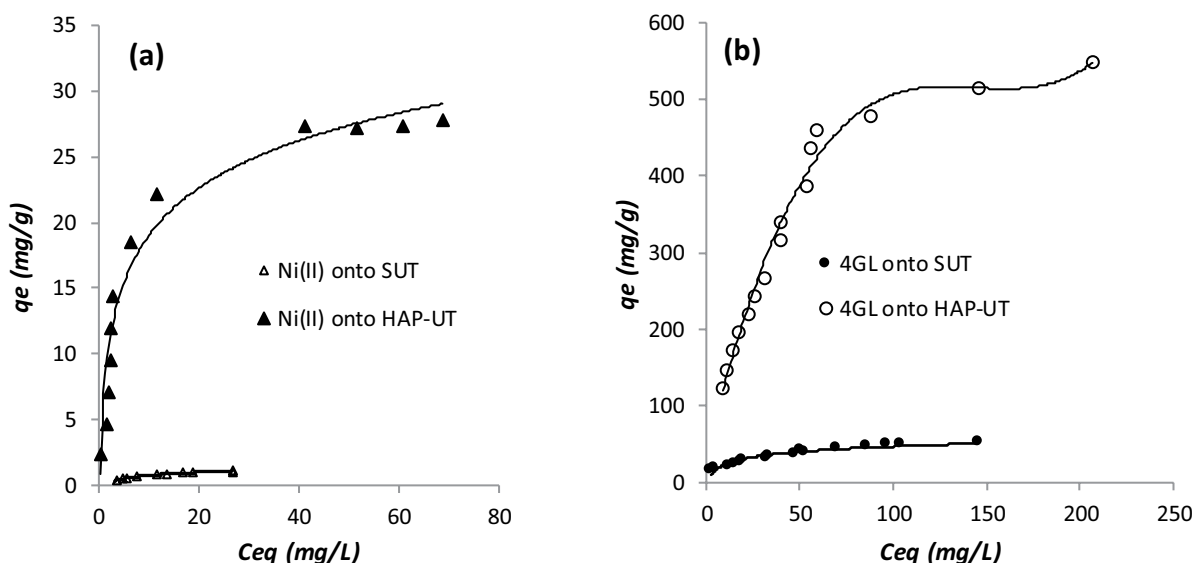| | | Pollutants | | | |
| | | Nickel ions | | Yellow supranol | |
| Model | Parameters | SUT | HAP-UT | SUT | HAP-UT |
| --- | --- | --- | --- | --- | --- |
| Langmuir | $R^2$ | 0.9886 | 0.9956 | 0.9807 | 0.9894 |
| | $b$ (mg g$^{-1}$) | 1.489 | 29.50 | 58.479 | 666.67 |
| | $K_L$ (L mg$^{-1}$) | 0.102 | 0.244 | 0.043 | 0.026 |
| | RMSE | 0.664 | 0.094 | 0.122 | 1.549 |
| Freundlich | $R^2$ | 0.9748 | 0.9025 | 0.9731 | 0.9339 |
| | $n$ | 0.221 | 1.002 | 2.729 | 2.057 |
| | $K_F$ (mg g$^{-1}$) | 1.98 | 5.247 | 8.623 | 50.249 |
| | RMSE | 18.678 | 1.990 | 0.0778 | 0.132 |



Fig. 5. Adsorption isotherms (a) nickel ion and (b) Supranol yellow (4GL) onto HAP-UT and SUT.

and SUT adsorbents are all favorable except for Ni ions which are poorly adsorbed ($n \leq 1$). From the perspective of the coefficient of determination, Langmuir model is more representative for the experimental data predicting homogeneous surface coverage of the adsorbent as pollutants concentration approaches saturation since their $R^2$ are higher compared to Freundlich isotherms in its linear form with lower root mean square error (RMSE) values. Maximum capacities obtained from linear Langmuir isotherms plots (Fig. 6b) are 666.67 and 58.48 mg g$^{-1}$ for 4GL dye and 29.50 and 1.49 mg g$^{-1}$ for Ni$^{2+}$ onto respectively HAP-UT and SUT. Maximum uptake values are lower for Ni$^{2+}$ especially onto the raw material, suggesting that electrostatic interaction and consequent bond between this metal and both adsorbents adsorption sites are weaker; the same finding has been reported in the literature [33–38]. Compared to other adsorbents reported in the literature and summarized in Table 4, implying that the hydroxyapatite obtained from sea urchin test (*Paracentrotus lividus*) as a waste can be efficiently used in removing dyes and metal ions as pollutants from wastewater.

### 3.4. Modeling of adsorption kinetics

In general, diffusion-controlled and adsorption-controlled models are mainly used to evaluate the equilibrium time and to describe the kinetic mechanism of adsorption process. In particular, the Lagergren pseudo-first-order, pseudo-second-order and intraparticle diffusion models in their linear forms were used in this study to the experimental data of Ni$^{2+}$ and Supranol yellow dye uptakes onto *Paracentrotus lividus*.

#### 3.4.1. Lagergren's equation

The original adsorption-controlled model of Lagergren also known as the pseudo-first-order model given by Eq. (9) is one of the most widely used for the adsorption of solute from a liquid solution.

$$\log\left(q_e - q_t\right) = \log q_{e,1} - \frac{k_1}{2.303}t \tag{9}$$

where $q_e$ and $q_t$ (mg g$^{-1}$) are the amount of pollutant adsorbed at equilibrium and at time $t$ (min), respectively, $k_1$ (min$^{-1}$)
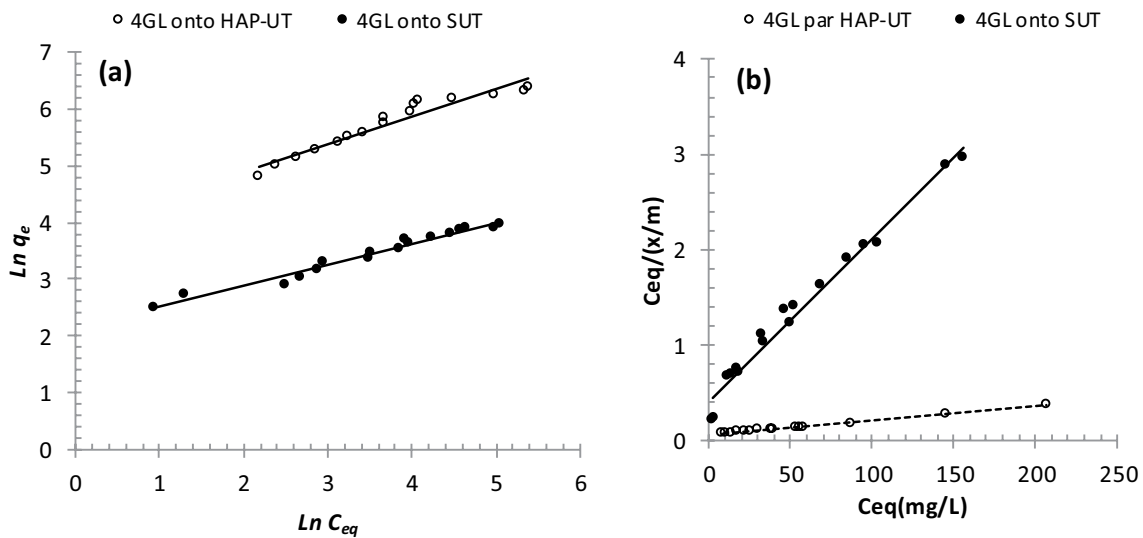


Fig. 6. (a) Freundlich and (b) Langmuir isotherm for Supranol yellow (4GL) onto HAP-UT and SUT adsorbents.

Table 4
Maximum adsorption capacities of various adsorbents for 4GL and Ni$^{2+}$ removal from liquid effluents

| Pollutants | Adsorbents | Maximum uptake (mg g$^{-1}$) | References |
|---|---|---|---|
| Ni$^{2+}$ | Algal species based activated carbon | 64.51 | [11] |
| | Aldrich activated carbon | 11.60 | [11] |
| | Nano-bentonite | 26.005 | [39] |
| | Olive stones waste | 39.06 | [40] |
| | Nanocrystallite hydroxyapatite | 18.6 | [36] |
| | Urchin test based-hydroxyapatite | 29.50 | This study |
| 4GL dye | Algal species based activated carbon | 625.00 | [9] |
| | Merck activated carbon | 84.03 | [9] |
| | Cr-intercalated montmorillonite | 58.47 | [8] |
| | Urchin test based-hydroxyapatite | 666.67 | This study |

is the pseudo-first-order adsorption rate constant, $t$ (min) is the contact time. Values of $q_e$ and $k_1$ determined from the intercept and slope of $\log(q_e - q_t)$ vs. $t$ plots are summarized in Table 5.

Adsorption of both pollutants data do not obey the pseudo-first-order model in its linear form since $R^2$ values are lower and also there is disagreement between the

Table 5
Kinetic parameters for the adsorption of Ni$^{2+}$ and 4GL dye onto prepared samples

| Pollutants | Nickel ions | | Supranol yellow | |
|---|---|---|---|---|
| Adsorbents | HAP-UT | SUT | HAP-UT | SUT |
| Initial concentration (mg L$^{-1}$) | 50 | 30 | 600 | 660 |
| Pseudo-first-order | | | | |
| $q_{e(exp)}$ (mg g$^{-1}$) | 3.587 | 1.666 | 148.82 | 5.79 |
| $q_{e(calc)}$ (mg g$^{-1}$) | 0.530 | 0.978 | 0.933 | 0.978 |
| $k_1$ (min$^{-1}$) | 0.636 | 0.020 | 0.069 | 0.023 |
| $R^2$ | 0.832 | 0.966 | 0.873 | 0.963 |
| RMSE | 0.724 | 22.933 | 0.554 | 0.238 |
| Pseudo-second-order | | | | |
| $q_{e(calc)}$ (mg g$^{-1}$) | 3.604 | 1.7182 | 149.254 | 5.903 |
| $q_{e(exp)}$ (mg g$^{-1}$) | 3.587 | 1.6656 | 148.82 | 5.79 |
| $k_2$ (g mg$^{-1}$ min$^{-1}$) | 0.402 | 0.098 | 0.0112 | 0.428 |
| $h$ (mg g$^{-1}$ min$^{-1}$) | 5.219 | 0.289 | 250.00 | 1.491 |
| $R^2$ | 0.9999 | 0.9986 | 1.000 | 0.9997 |
| RMSE | 0.132 | 1.008 | 0.001 | 0.173 |
| Intraparticle diffusion | | | | |
| $k_{int}$ (mg g$^{-1}$ min$^{-0.5}$) | 0.0339 | 0.046 | 0.451 | 0.0742 |
| $C$ (mg g$^{-1}$) | 3.2594 | 1.159 | 144.17 | 4.8562 |
| $R^2$ | 0.9140 | 0.9636 | 0.9674 | 0.9666 |

experimental ($q_{e,experimental}$) equilibrium adsorption capacities and the calculated ones ($q_{e,calculated}$). Hence, adsorption might not be diffusion-controlled phenomena.

### 3.4.2. Pseudo-second-order equation

Actually, the pseudo-second-order equation, developed by Ho and Mckay given by Eq. (10), is probably the most popular model used to describe adsorption kinetics, especially for new and novel sorbent materials [41,42].

$$\frac{t}{q_t} = \frac{1}{k_2 q_{e,2}^2} + \frac{1}{q_e} t \tag{10}$$

where $k_2$ (g mg$^{-1}$ min$^{-1}$) is the rate constant of the second-order equation. $q_e$ and $k_2$ determined from the intercept and slope $t/q_t$ vs. $t$ plots.

As shown in Fig. 7a and b, and in contrast to the pseudo-first-order, the pseudo-second-order model is very representative for all Supranol yellow and Ni$^{2+}$ adsorption data in their linear forms since $q_{e(exp)}$ and $q_{e(calc)}$ match closely and $R^2$ values are close to unity.

Same finding were reported in the literature using different adsorbents [9,11,40], which indicated that the rate-limiting step of adsorption process might be the chemisorption, involving valence forces through sharing or exchange or of electrons between HAP-UT and Ni$^{2+}$.

### 3.4.3. Intraparticle diffusion

The intraparticle diffusion model proposed by Weber–Morris given by Eq. (11) widely applied for the analysis of adsorption kinetics, is used in this study to interpret experimental kinetics data, from a mechanistic viewpoint. The $q_t$ vs. $t^{0.5}$ plots may theoretically present one straight line in which the intraparticle diffusion is alone the rate limiting step or multi-linearity indicating then; the overall adsorption process may be controlled either by more than one step, such as film or external diffusion, pore diffusion,
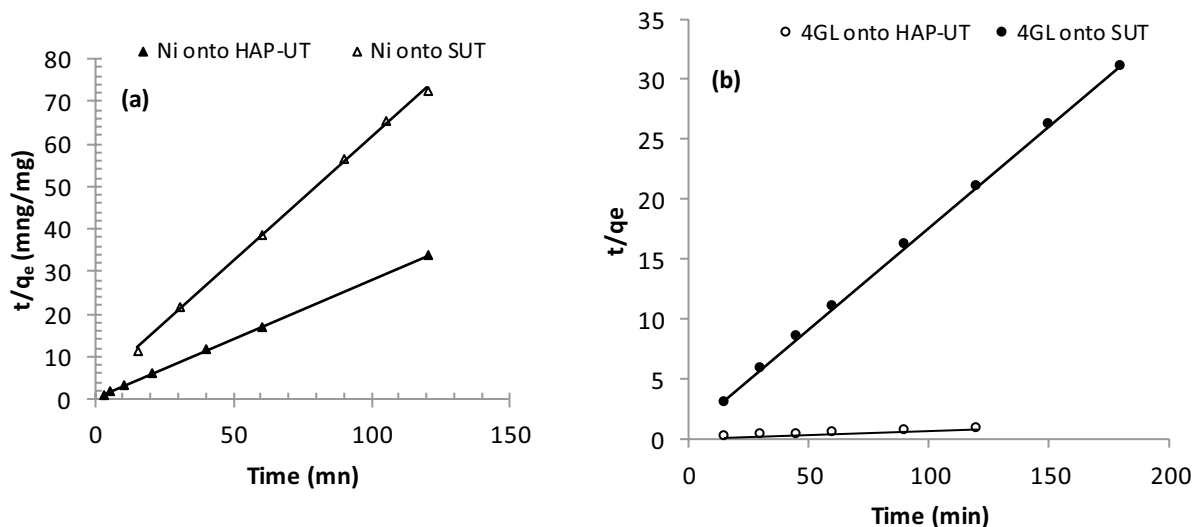


Fig. 7. Pseudo-second-order adsorption kinetics of (a) Ni$^{2+}$ and (b) 4GL, onto HAP-UT and SUT samples.

surface diffusion and adsorption on the pore surface, or a combination of at least two steps.

$$q_t = k_{int}\sqrt{t} + C \tag{11}$$

where $k_{int}$ (mg g$^{-1}$ min$^{-1/2}$) is the intraparticle diffusion rate constant, and $C$ (mg g$^{-1}$) is a constant related to the thickness of the boundary layer. $C$ is the intercept, it determines the boundary layer effect (higher values, the greater the effect) and $k_{int}$ is the slope determined from Weber–Morris plots ($q_t$ vs. $t^{0.5}$).

From results presented in Table 5 and plotted in Fig. 8a and b, we can see that there are one straight lines with good fitting (higher $R^2$ values) for considered cases which do not pass through the origin, which means that the intraparticle diffusion does not control the adsorption process in accordance with the positive $C$ values. The $C$ values which give an idea on the thickness of the boundary layer are all positive ($C \neq 0$) for all considered systems implying that the intraparticle diffusion mechanism does not solely limit the overall adsorption process, but it is involved since $q_t$ vs. $t^{0.5}$ plots gave Straight lines.

*3.5. Errors analysis*

In addition to $R^2$ values, an error function is to be defined as an optimization procedure requirement for evaluating the single-component isotherm and kinetics studies to the experimental equilibrium data. In this study, the residual RMSE given by Eq. (12) was used for this purpose.

$$RMSE = \sqrt{\left(\frac{1}{N-2}\right) \times \sum_{1}^{N}\left(q_{e,exp} - q_{e,cal}\right)^2} \tag{12}$$

The small the RMSE value, the better the curve fitting. In general low values of errors function means more there is an agreement between the experimental and calculate data and more the model converge and becomes favourable which is the case of the presented isotherm and kinetics values in Tables 3 and 5 respectively

*3.6. Thermodynamic study*

*3.6.1. Van't Hoff equation*

The distribution coefficient method using Eq. (4) is widely used for calculating thermodynamic parameters. The main concern is the units of $K_d$ in this equation are L g$^{-1}$. It is not appropriate to use $K_d$ values directly for $\Delta G°$, $\Delta H°$ and $\Delta S°$ calculations. Thus, $K_d$ should be dimensionless coefficient. To do so, we use the molecular weight of adsorbate (g mol$^{-1}$) and the number of moles of pure water per litter (mol L$^{-1}$) as multiplying factor of $K_d$ in L g$^{-1}$. The obtained values are presented in Table 6. Fig. 9a shows
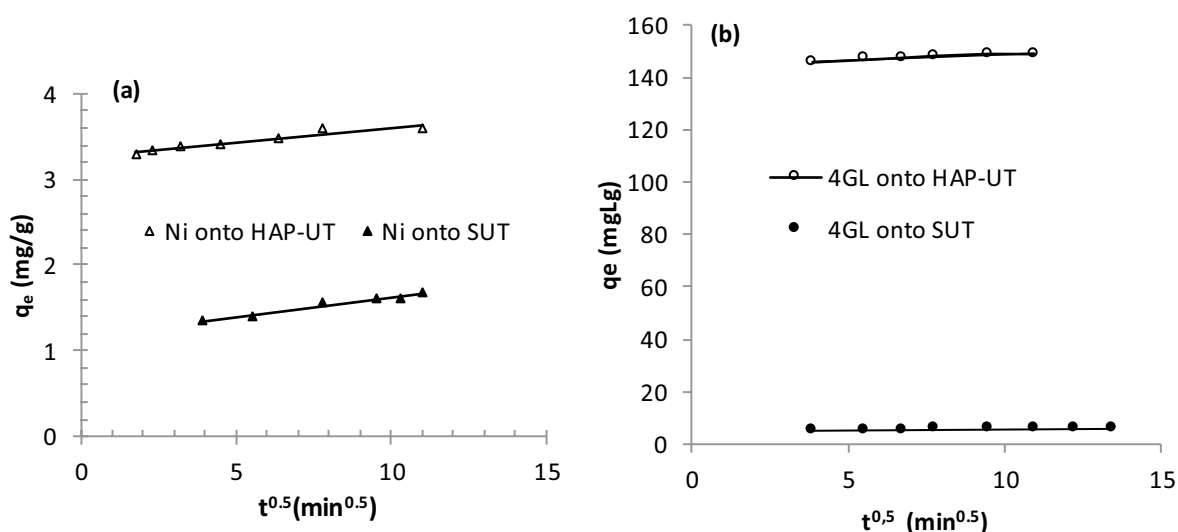


Fig. 8. Intraparticle diffusion for (a) Ni$^{2+}$ and (b) 4GL, onto HAP-UT and SUT samples.

Table 6
Comparison of distribution coefficient $K_d$ (dimension and dimensionless values)

| Temperature (K) | | $K_d$ (L g$^{-1}$) | | | $K_d$ (dimensionless) | | |
|---|---|---|---|---|---|---|---|
| | | 298 | 303 | 313 | 298 | 303 | 313 |
| HAP-UT | Ni(II) | 0.30756 | 0.55322 | 1.12576 | 1,001.928 | 1,802.097 | 3,667.154 |
| | 4GL | 3.93169 | 6.114740 | 9.30303 | 98,630.475 | 153,394.377 | 233,375.818 |
| SUT | Ni(II) | 0.1149 | 0.1386 | 0.1881 | 374.214 | 451.538 | 612.764 |
| | 4GL | 0.18375 | 0.253783 | 0.48717 | 4,394.349 | 6,468.036 | 12,221.173 |

plots of $\ln K_{d(dimensionless)}$ vs. $T^{-1}$ from which $\Delta S°$ and $\Delta H°$ are obtained from the intercept and the slope respectively using Eqs. (5) and (6).

Thermodynamic functions values are summarized in Table 7. Negative values of $\Delta G°$ indicate that nature of 4GL Ni ions adsorption onto HAP-UT and SUT samples at different temperatures is spontaneous. Also, the negative values of $\Delta H°$ and their magnitude in all cases are both indications that adsorption processes were taken place via physisorption associated with exothermicity. The positive values of $\Delta S°$ indicate the increased randomness at the adsorbent–adsorbate interface during the adsorption process and as good affinity of nickel ions and Supranol yellow dye toward HAP-UT and SUT adsorbents.

### 3.6.2. Modified Arrhenius-type equation

The activation energy and the sticking coefficient values are evaluated from the slope and the intercept of $\ln(1-\theta)$ vs. $(1/T)$ plots represented by Fig. 9b. The estimated activation energies, from the plots with good fitting are shown in Table 7.

Comparable with $\Delta H°$, the positive values of $E_a$ and their magnitudes confirm the endothermicity and the physical nature of $Ni^{2+}$ and 4GL removal by HAP-UT and SUT. Defined as a measure of the potential of a sorbate to remain on the sorbent indefinitely and depending on the

system temperature, $S^*$ values were estimated in the range of 25°C–45°C based on the surface coverage at this range of temperature as shown in Table 7. These results suggest that the probability of both pollutants to stick very well to the HAP-UT and SUT surfaces since $S^* \ll 1$, confirming that the adsorption processes are effectively physical ones (mechanism of physisorption is dominant) as explained below:

The same finding was reported in the literature [43].

### 4. Conclusion

This research confirmed that *Paracentrotus lividus* based-hydroxyapatite can be efficiently used as an adsorbent to remove nickel ions and Yellow supranol dye for up to respectively 29.50 and 666.67 mg g$^{-1}$ from simulated water at quick equilibrium time of about 40 min. The conversion of sea urchin test (SUT), an affordable biomaterial into hydroxyapatite-based adsorbent (HAP-UT) using simultaneous action (chemical and heat) enhances considerably the specific surface area of about 80% relative to its inactivated state. Pseudo-second-order kinetics was confirmed for both pollutants adsorption and Langmuir model was found to better describe them. Thermodynamic study indicated that the adsorption processes were endothermic and spontaneous. The physical mechanism is the dominant adsorption process. Obtained results suggest that the probability of both pollutants to stick very well

| Sticking coefficient | Mechanism |
|---|---|
| $S^* > 1$ | Sorbate unsticking to sorbent: weak adsorption exist |
| $S^* = 1$ | Linear sorbate-sorbent relation of sticking exists: existence of both chemisorption and physisorption mechanisms |
| $S^* = 0$ | Indefinite sticking of sorbate to sorbent: chemisorption mechanism is dominant |
| $0 < S^* < 1$ | Favourable sticking of sorbate to sorbent: physisorption mechanism is dominant |
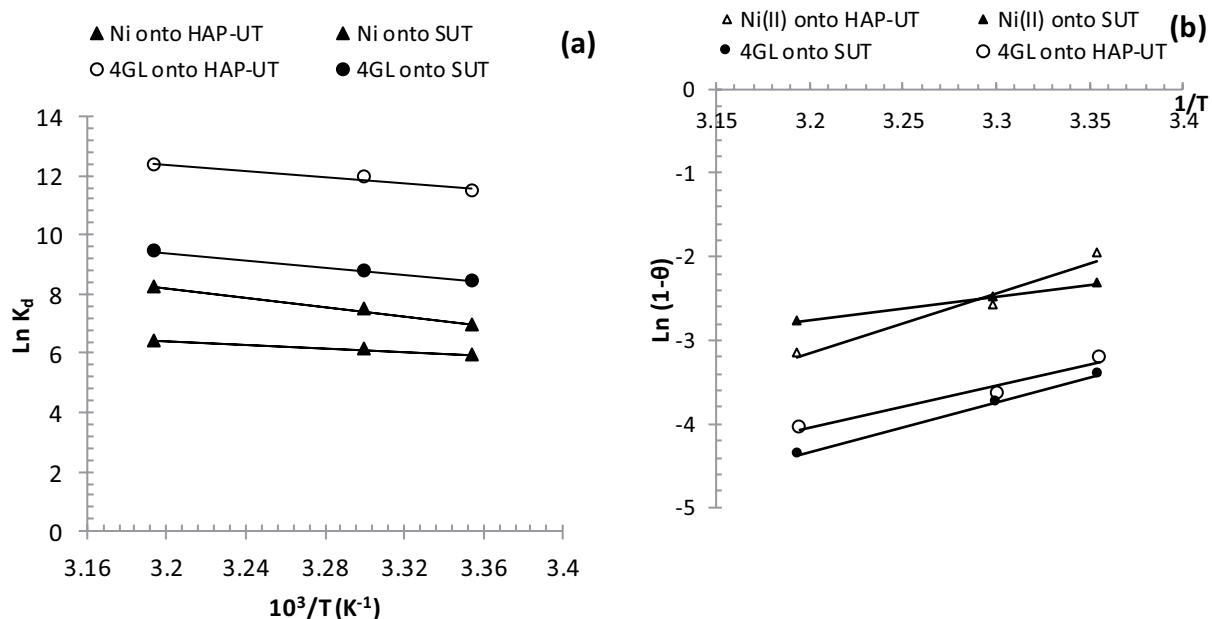


Fig. 9. (a) Van't Hoff and (b) modified Arrhenius plots for Ni(II) and 4GL adsorption.

Table 7
Thermodynamic parameters of Ni$^{2+}$ and Supranol yellow adsorption

| Adsorbents | Pollutants | $R^2$ | $-\Delta H°$ (kJ mol$^{-1}$) | $\Delta S°$ (kJ mol$^{-1}$) | $-\Delta G°$ (kJ mol$^{-1}$) | | | $E_a$ (kJ mol$^{-1}$) | $S*$ |
|---|---|---|---|---|---|---|---|---|---|
| | | | | | 298 K | 303 K | 313 K | | |
| HAP-UT | Ni(II) | 0.9850 | 65.6846 | 0.3357 | 17.128 | 18.895 | 21.369 | 59.48 | $4.87 \times 10^{-12}$ |
| | 4GL | 0.9634 | 43.0610 | 0.2979 | 28.504 | 30.095 | 32.181 | 41.95 | $1.75 \times 10^{-9}$ |
| SUT | Ni(II) | 0.9983 | 25.3328 | 0.1917 | 14.687 | 15.405 | 16.709 | 23.35 | $7.90 \times 10^{-6}$ |
| | 4GL | 1.000 | 50.2007 | 0.2972 | 20.903 | 22.115 | 24.502 | 49.48 | $1.01 \times 10^{-11}$ |

to the HAP-UT and SUT surfaces ($S* \ll 1$), supported by the activation energy ($E_a$), they confirm that the mechanism of physisorption is dominant. It may be concluded that HAP-UT as a synthesized adsorbent from sea urchin test (SUT), can be used as an alternative to the costly commercial adsorbents in recovering dyestuff and heavy metals from industrial wastewater.

## Declaration of interests

The authors declare that they have no known competing financial interests or personal relationships that could have appeared to influence the work reported in this paper.

## Acknowledgment

## References

[1] S. Mandal, A. Kunhikrishnan, N.S. Bolan, H. Wijesekara, R. Naidu, Chapter 4 – Application of Biochar Produced From Biowaste Materials for Environmental Protection and Sustainable Agriculture Production, M.N.V. Prasad, K. Shih, Eds., Environmental Materials and Waste, Academic Press, London, 2016, pp. 73–89.

[2] J. Briffa, E. Sinagra, R. Blundell, Heavy metal pollution in the environment and their toxicological effects on humans, Heliyon, 6 (2020) e04691, doi: 10.1016/j.heliyon.2020.e04691.

[3] V. Masindi, K.L. Muedi, Environmental Contamination by Heavy Metals, Heavy Metals, H. El-Din, M. Saleh, R.F. Aglan, IntechOpen, 2018, doi: 10.5772/intechopen.76082. Available at: https://www.intechopen.com/chapters/60680

[4] A.R. Wuana, F.E. Okieimen, Heavy metals in contaminated soils: a review of sources, chemistry, risks and best available strategies for remediation, Int. Sch. Res. Network ISRN Ecol., 2011 (2011) 402647, 20 pages, doi: 10.5402/2011/402647.

[5] K. Hunger, Industrial Dyes: Chemistry, Properties, Applications, Wiley-VCH: Verlag GmbH & Co. KGaA, Weinheim, 2003.

[6] B. Senthil Rathi, P. Senthil Kumar, Application of adsorption process for effective removal of emerging contaminants from water and wastewater, Environ. Pollut., 280 (2021) 116995, doi: 10.1016/j.envpol.2021.116995.

[7] C. Tien, Introduction to Adsorption: Basics, Analysis, and Applications, 50 Hampshire Street, 5th Floor, Cambridge, MA 02139, Elsevier, United States, 2019.

[8] Z. Bouberka, A. Khenifi, N. Benderdouche, Z. Derriche, Removal of Supranol yellow 4GL by adsorption onto Cr-intercalated montmorillonite, J. Hazard. Mater. B, 133 (2006) 154–161.

[9] F. Nemchi, B. Bestani, N. Benderdouche, M. Belhakem, L. Charles de Minorval, Adsorption of Supranol yellow 4GL from aqueous solution onto activated carbons prepared from seawater algae, Adsorpt. Sci. Technol., 30 (2012) 81–95.

[10] N. Benderdouche, B. Bestani, B. Benstaali, Z. Derriche, Enhancement of the adsorptive properties of a desert *Salsola vermiculata* species, Adsorpt. Sci. Technol., 21 (2003) 739–750.

[11] F. Nemchi, B. Bestani, N. Benderdouche, M. Belhakem, L. Duclaux, Enhancement of Ni$^{2+}$ removal capacity of activated carbons obtained from Mediterranean *Ulva lactuca* and *Systoceira stricta* algal species, J. Environ. Chem. Eng., 5 (2017) 2337–2345.

[12] S. George, D. Mehta, V.K. Saharan, Application of hydroxyapatite and its modified forms as adsorbents for water defluoridation: an insight into process synthesis, Rev. Chem. Eng., 36 (2020) 369–400.

[13] G. Ma, Three common preparation methods of hydroxyapatite, IOP Conf. Ser.: Mater. Sci. Eng., 688 (2019) 033057.

[14] S.L. Iconaru, M. Motelica-Heino, R. Guegan, M. Beuran, A. Costescu, D. Predoi, Adsorption of Pb(II) ions onto hydroxyapatite nanopowders in aqueous solutions, Materials (Basel), 11 (2018) 2204, doi: 10.3390/ma11112204.

[15] S.M. Mousa, N.S. Ammar, H.A. Ibrahim, Removal of lead ions using hydroxyapatite nano-material prepared from phosphogypsum waste, J. Saudi Chem. Soc., 20 (2016) 357–365.

[16] D.C. Manatunga, R.M. de Silva, K.M. Nalin de Silva, R. Ratnaweera, Natural polysaccharides leading to super adsorbent hydroxyapatite nanoparticles for the removal of heavy metals and dyes from aqueous solutions, RSC Adv., 6 (2016) 105618–105630.

[17] E. Kusrini, N. Sofyan, D.M. Nurjaya, S. Santoso, D. Tristantini, Removal of heavy metals from aqueous solution by hydroxyapatite/chitosan composite, Adv. Mater. Res., 789 (2013) 176–179.

[18] N.T. Thom, D.T.M. Thanh, P.T. Nam, N.T. Phuong, C. Buess-Herman, Adsorption behavior of Cd$^{2+}$ ions using hydroxyapatite (HAp) powder, Green Process. Synth., 7 (2018) 409–416.

[19] N.A.S. Mohd Pu'ad, R.H. Abdul Haq, H. Mohd Noh, H.Z. Abdullah, M.I. Idris, T.C. Lee, Synthesis method of hydroxyapatite: a review, Mater. Today: Proc., 29 (2020) 233–239.

[20] M. Kalbarczyk, A. Szcześ, D. Sternik, The preparation of calcium phosphate adsorbent from natural calcium resource and its application for copper ion removal, Environ. Sci. Pollut. Res., 28 (2021) 1725–1733.

[21] G. Charlot, Dosages absorptiomètriques des éléments minéraux, 3$^{eme}$ edition, Masson, 1978.

[22] B. Natesh Kumar, S. Kanchi, M.I. Sabela, K. Bisetty, N.V.V. Jyothi, Spectrophotometric determination of nickel(II) in waters and soils: novel chelating agents and their biological applications supported by DFT method, Karbala Int. J. Mod. Sci., 2 (2016) 239–250.

[23] M. Benzekri Benallou, N. Douara, M.A. Chemrak, Z. Mekibes, N. Benderdouche, B. Bestani, Elimination of Malachite Green on granular activated carbon prepared from olive stones in discontinuous and continuous modes, Algerian J. Environ. Sci. Technol., 7 (2021) 1698–1706.

[24] Z. Mekibes, B. Bestani, N. Douara, N. Benderdouche, M. Benzekri-Benallou, Simultaneous activation of *Ficus carica* L. leaves for the removal of emerging pollutants from aqueous solutions, Desal. Water Treat., 222 (2021) 322–335.

[25] O. Douinat, B. Bestani, N. Benderdouche, A. Boucherdoud, Use of *Olea europaea* leaves-based activated carbon for pollutant removal from liquid effluents, Desal. Water Treat., 210 (2021) 258–272.

[26] D.Z. Marković-Nikolić, M.D. Cakić, G. Petković, G.S. Nikolić, Kinetics, thermodynamics and mechanisms of phosphate sorption onto bottle gourd biomass modified by (3-chloro-2-hydroxypropyl) trimethylammonium chloride, Prog. React. Kinet. Mech., 44 (2019) 267–285.

[27] K.S.W. Sing, D.H. Everett, R.A.W. Haul, L. Moscou, R.A. Pierotti, J. Rouquerol, T. Siemieniewska, Reporting physisorption data for gas/solid systems with special reference to the determination of surface area and porosity (Recommendations 1984), Pure Appl. Chem., 57 (1985) 603–619.

[28] S. Yanyan, W. Guangxin, S. Guoqing, W. Yaming, L. Wuhui, A. Osaka, Effects of amino acids on conversion of calcium carbonate to hydroxyapatite, RSC Adv., 10 (2020) 37005–37013.

[29] H. Mahroug, A. Mansri, F. Dergal, The effect of calcium suspension concentration on the hydroxyl-apatite structures and purity, Rev. Roum. Chim., 64 (2019) 277–286.

[30] J.C. Elliott, R.M. Wilson, S.E.P. Dowker, Apatite structures. JCPDS-international centre for diffraction data, Adv. X-ray Anal., 45 (2002).

[31] A.B. Hazar Yoruça, A. Karakaş Aydınoğlu, E. Ayas, A. Koyun, Effect of precipitation method on properties of hydroxyapatite powders, Proc. Acta Phys. Pol., A, 123 (2013) 371–373.

[32] J.H. Shariffuddin, M.I. Jones, D.A. Patterson, Greener photocatalysts: hydroxyapatite derived from waste mussel shells for the photocatalytic degradation of a model azo dye wastewater, Chem. Eng. Res. Des., 91 (2013) 1693–1704.

[33] A. Khenifi, Z. Bouberka, F. Sekrane, M. Kameche, Z. Derriche, Adsorption study of an industrial dye by an organic clay, Adsorption, 13 (2007) 149–158.

[34] L.P. Cruz-Lopes, M. Macena, B. Esteves, R.P.F. Guiné, Ideal pH for the adsorption of metal ions $Cr^{6+}$, $Ni^{2+}$, $Pb^{2+}$ in aqueous solution with different adsorbent materials, Open Agric., 6 (2021) 115–123.

[35] H. Çelebi, G. Gök, O. Gök, Adsorption capability of brewed tea waste in waters containing toxic lead(II), cadmium(II), nickel(II), and zinc(II) heavy metal ions, Sci. Rep., 10 (2020) 17570, doi: 10.1038/s41598-020-74553-4.

[36] M. Ferri, S. Campisi, A. Gervasini, Nickel and cobalt adsorption on hydroxyapatite: a study for the de-metalation of electronic industrial wastewaters, Adsorption, 25 (2019) 649–660.

[37] S. Campisi, C. Castellano, A. Gervasini, Tailoring the structural and morphological properties of hydroxyapatite materials to enhance the capture efficiency towards copper(II) and lead(II) ions, New J. Chem., 42 (2018) 4520–4530.

[38] L. Silvester, J.-F. Lamonier, R.-N. Vannier, C. Lamonier, M. Capron, A.-S. Mamede, F. Pourpoint, A. Gervasini, F. Dumeignil, Structural, textural and acid-base properties of carbonates-containing hydroxyapatites, J. Mater. Chem. A, 2 (2014) 11073–11090.

[39] A.A. Taha, A.M. Ahmed, H.H. Abdel Rahman, F.M. Abouzeid, M.O. Abdel Maksoud, Removal of nickel ions by adsorption on nano-bentonite: equilibrium, kinetics, and thermodynamics, J. Dispersion Sci. Technol., 38 (2017) 757–767.

[40] M. Corral Bobadilla, R. Lostado Lorza, F. Somovilla Gómez, R. Escribano García, Adsorptive of nickel in wastewater by olive stone waste: optimization through multi-response surface methodology using desirability functions, Water, 12 (2020) 1320, doi: 10.3390/w12051320.

[41] M.A. Hubbe, A. Azizian, S. Douven, Implications of apparent pseudo-second-order adsorption kinetics onto cellulosic materials: a review, BioResouces, 14 (2019) 7582–7626.

[42] J. Bullen, S. Saleesongsom, D.J. Weiss, A revised pseudo-second-order kinetic model for adsorption, sensitive to changes in sorbate and sorbent concentrations, Langmuir, 37 (2021) 3189–3201.

[43] S. Gupta, A. Kumar, Removal of nickel(II) from aqueous solution by biosorption on *A. barbadensis Miller* waste leaves powder, Appl. Water Sci., 9 (2019) 1–11, doi: 10.1007/s13201-019-0973-1.